Investigation by EPR and ENDOR Spectroscopy of the Nickel(I) Form of Cofactor F_{430}[1] of *Methanobacterium thermoautotrophicum* and of Nickel(I) Octaethylisobacteriochlorin

Joshua Telser,[†,||] Yang-Cheng Fann,[†] Mark W. Renner,[§] Jack Fajer,[§] Shengke Wang,[‡,⊥] Hui Zhang,[‡] Robert A. Scott,*[,‡] and Brian M. Hoffman*[,†]

Contribution from the Department of Chemistry, Northwestern University, Evanston, Illinois 60208-3113, Center for Metalloenzyme Studies, University of Georgia, Athens, Georgia 30602-2556, and Department of Applied Science, Brookhaven National Laboratory, Upton, New York 11973-5000

Received July 23, 1996[⊗]

Abstract: The terminal step in methane generation by the archaeon *Methanobacterium thermoautotrophicum* is catalyzed by the enzyme *S*-methyl coenzyme M reductase (methylreductase). This enzyme contains a Ni(II) tetrapyrrole cofactor, F_{430}, at the active site in the resting state. A Ni(I) state (Ni^IF_{430}) has been proposed as the active form of the cofactor. Nickel isobacteriochlorins have been used to model F_{430}. We have investigated both Ni^IF_{430} and Ni^IOEiBC using CW and pulsed EPR and ENDOR spectroscopy at X-band and Q-band microwave frequencies. In agreement with a previous X-band EPR and ESEEM study, at Q-band, the **g** tensor of Ni^IF_{430} appears axial and ^{1,2}H ENDOR of Ni^IF_{430} in H_2O versus D_2O solvent shows no evidence for strongly coupled, solvent-exchangeable hydrogens, and this indicates that there is no water axially coordinated to Ni(I) in contrast to the Ni(II) resting state. Both Ni^IF_{430} and Ni^IOEiBC give ^{14}N ENDOR signals arising from the four pyrrole nitrogen ligands to Ni(I). Previous EXAFS studies of Ni^IOEiBC and $Ni^IF_{430}Me_5$ showed two sets of Ni(I)−N distances differing by ∼8%, and in agreement with this, the ^{14}N ENDOR signals for both Ni^IOEiBC and Ni^IF_{430} can be analyzed in terms of superimposed signals from two distinct types of nitrogen ligand. The difference in bond lengths determined by EXAFS is reflected in different hyperfine and quadrupole coupling constants as determined by ENDOR. Comparison of these magnetic parameters for Ni(I) complexes with those for related species, such as Cu^{II}TPP, shows that one set of nitrogen ligands resembles porphyrin pyrrole, while the other set is distinctively different.

Introduction

Methanogens are a class of strictly anaerobic archaea, many of which are capable of living autotrophically on hydrogen and carbon dioxide.[2] They derive energy from the stepwise reduction of carbon dioxide to methane.[3] The final step in this catalytic C_1 chemistry is the reductive cleavage of *S*-methyl coenzyme M to coenzyme M and methane.[4−6] The reaction is catalyzed by *S*-methyl coenzyme M reductase (methylreductase), which has been isolated from *Methanobacterium thermoautotrophicum* (strains ΔH and Marburg).[7,8] Methylreductase is a large, complex enzyme of ∼300 kDa with an $\alpha_2\beta_2\gamma_2$ subunit structure.[7,8] Each α subunit contains a tightly bound cofactor, F_{430}, that has been shown to be a Ni(II) tetrapyrrole derivative.[9,10] The structure of native F_{430} has been determined by a variety of spectroscopic techniques and is shown in Figure 1. The significantly nonplanar geometry of F_{430} is shown in Chart 1. The model was generated from the crystallographic data for $Ni^{II}F_{430}Me_5$;[9] for clarity, no side chains are shown except for the cyclohexanone fused to ring D.

† Northwestern University.
‡ University of Georgia.
§ Brookhaven National Laboratory.
|| Permanent address: Chemistry Program, Roosevelt University, 430 S. Michigan Ave., Chicago, IL 60605-1394.
⊥ Current address: Center for Synchrotron Radiation Research and Instrumentation, Department of Physics, Illinois Institute of Technology, Chicago, IL 60616.
* Address correspondence to these authors at the following addresses: B.M.H., Department of Chemistry, Northwestern University, 2145 Sheridan Road, Evanston, IL 60208-3113. Voice: (847) 491-3104. FAX: (847) 491-7713. Internet: bmh@nwu.edu. R.A.S., Center for Metalloenzyme Studies, University of Georgia, Athens, GA 30602-2556. Voice: (706) 542-2240. FAX: (706) 542-9454. Internet: scott@bscr.uga.edu.
⊗ Abstract published in *Advance ACS Abstracts,* January 15, 1997.
(1) Abbreviations used: F_{430}, nickel tetrapyrrole pentacarboxylic acid cofactor; methyl coenzyme M, $F_{430}Me_5$, nickel tetrapyrrole pentamethyl ester cofactor; 2-(methylthio)ethanesulfonic acid; OEiBC, octaethylisobacteriochlorin (*tct*-2,3,7,8-tetrahydro-2,3,7,8,12,13,17,18-octaethylporphyrin dianion); TPP, 5,10,15,20-tetraphenylporphyrin dianion; TPiBC, tetraphenylisobacteriochlorin (*tct*,*ttt*-2,3,7,8-tetrahydro-5,10,15,20-tetraphenylporphyrin dianion); Me_6[14]1,4,8,11-tetraeneN_4, 5,7,7,12,14,14-hexamethyl-1,4,8,11-tetraazacyclotetradeca-1,4,8,11-tetraene; Me_6[14]4,11-dieneN4, 5,7,7,12,14,14-hexamethyl-1,4,8,11-tetraazacyclotetradeca-4,11-diene; CAPS, 3-(cyclohexylamino)-1-propanesulfonic acid; 2-Me-THF, 2-methyltetrahydrofuran; Im, imidazole; SOD, superoxide dismutase; EPR, electron paramagnetic resonance; ENDOR, electron nuclear double resonance; CW, continuous wave; rf, radiofrequency; ESE, electron spin echo; ESEEM, electron spin echo envelope modulation; EXAFS, extended X-ray absorption fine structure; MCD, magnetic circular dichroism; NQR, nuclear quadrupole resonance; hwhm, half-width at half-maximum.

(2) Daniels, L.; Sparling, R.; Sprott, G. D. *Biochim. Biophys. Acta* **1984**, 113−163.
(3) Whitman, W. B. *Bacteria* **1985**, *8*, 2−84.
(4) Rouviere, P. E.; Wolfe, R. S. *J. Biol. Chem.* **1988**, *263*, 7913−7916.
(5) Wackett, L. P.; Honek, J. F.; Begley, T. P.; Shames, S. L.; Niederhoffer, E. C.; Hausinger, R. P.; Orme-Johnson, W. H.; Walsh, C. T. In *The Bioinorganic Chemistry of Nickel*; Lancaster, J. R., Jr., Ed.; VCH Publishers: New York, 1988.
(6) Wolfe, R. S. *Trends Biol. Sci.* **1985**, 396−399.
(7) Rospert, S.; Linder, D.; Ellermann, J.; Thauer, R. K. *Eur. J. Biochem.* **1990**, *194*, 871−877.
(8) Brenner, M. C.; Ma, L.; Johnson, M. K.; Scott, R. A. *Biochim. Biophys. Acta* **1992**, *1120*, 160−166.
(9) Färber, G.; Keller, W.; Kratky, C.; Jaun, B.; Pfaltz, A.; Spinner, C.; Kobelt, A.; Eschenmoser, A. *Helv. Chim. Acta* **1991**, *74*, 697−716.
(10) Won, H.; Olson, K. D.; Hare, D. R.; Wolfe, R. S.; Kratky, C.; Summers, M. F. *J. Am. Chem. Soc.* **1992**, *114*, 6880−6892.

S0002-7863(96)02533-4 CCC: $14.00

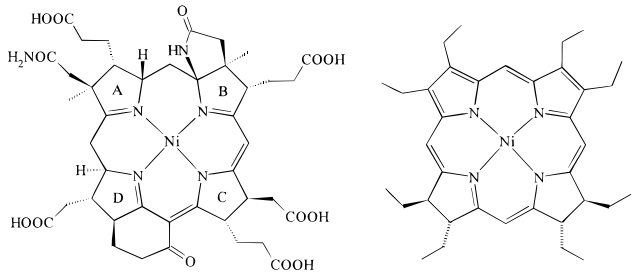

F_{430} $Ni^{II}OEiBC$ (*tct*)

Figure 1. Structures of the native form of F_{430}, as derived by spectroscopic and crystallographic analyses,[9,10] and of the *tct* isomer of $Ni^{II}OEiBC$. The conventional ring labels are indicated for F_{430}.

Chart 1

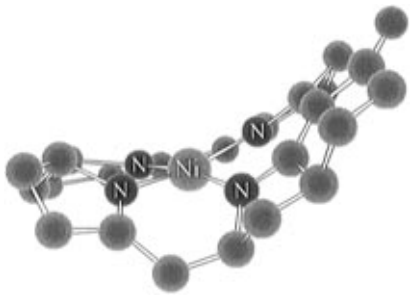

A model compound for the complex F_{430} macrocycle is the synthetically accessible octaethylisobacteriochlorin (OEiBC).[11−15] Synthesis yields a 1:1 mixture of two stereoisomers of the ligand, *trans*−*trans*−*trans* (*ttt*) and *trans*−*cis*−*trans* (*tct*), which can be separated by liquid chromatography.[16] The *tct* isomer of $Ni^{II}OEiBC$ is shown in Figure 1. This stereoisomer is thermodynamically more stable but has a smaller metal binding constant.[17−19]

F_{430} contains Ni(II) (pseudo-octahedral d^8, $S = 1$), but a Ni(I) (d^9, $S = {}^1/_2$) oxidation state is the likely catalytic transient.[7,8,20] Reductive activation of methylreductase can be achieved using Ti(III) citrate in place of the physiological reductant, and this electron donor will also reduce isolated F_{430} in alkaline aqueous solution.[21] $Ni^{II}OEiBC$ is readily reduced to the Ni(I) anion by sodium amalgam in dry THF,[11−13] in contrast to the behavior of Ni(II) complexes of other tetrapyrrole ligands, such as porphyrins and chlorins. The reduction of Ni(II) porphyrins is extremely sensitive to solvent, porphyrin ligand, temperature, and coordination of axial ligands, so that either Ni(II) porphyrin π anion radicals or Ni(I) porphyrin anions are formed, or a mixture of these two species.[14,22,23] Another notable point is that X-ray crystallographic and EXAFS studies of both F_{430}[24] and $Ni^{II}OEiBC$ showed that the four Ni(II)−N bond lengths are nearly identical,[9,15,17,25−27] whereas EXAFS studies of the corresponding Ni(I) forms, $Ni^{I}OEiBC$,[15] $Ni^{I}F_{430}$,[28] and $Ni^{I}F_{430}Me_5$,[27] indicated two inequivalent sets of Ni(I)−N bond lengths, differing by ∼0.15 Å (∼8%) for each complex. This divergence of Ni(I)−N bond lengths into two sets of distances, as determined in solution by EXAFS, is also a solid-state effect as demonstrated by several X-ray crystallographic studies of Ni(I) complexes with tetraazamacrocyclic ligands.[29−33] These studies show that, depending on the macrocyclic ligand's flexibility, reduction of Ni(II) to Ni(I) is associated with either expansion of the Ni−N distances, a distortion in the NiN_4 core, or both expansion and distortion.

Thus, nickel complexes of F_{430} and OEiBC are of interest for reasons of coordination chemistry as well as biochemistry. The paramagnetic Ni(I) complexes are amenable to investigation by electron nuclear double resonance (ENDOR) spectroscopy, which provides detailed information on electronic structure. We have therefore undertaken parallel ENDOR studies of $Ni^{I}F_{430}$, generated by Ti(III) citrate reduction in aqueous solution, and of $Ni^{I}OEiBC$, generated by Na reduction in 2-Me-THF solution. These ENDOR studies indeed help unravel the electronic structure of the complexes and provide evidence for inequivalence among the nitrogen ligands to Ni(I).

Experimental Section

Preparation of $Ni^{I}F_{430}$. Both native and 12,13-diepimeric forms of F_{430} were purified in the Ni(II) oxidation state as previously described.[34] On the time scale used here for reduction and sample preparation, there should be no conversion to the 12,13-diepimeric form of F_{430}.

Titanium(III) chloride was obtained from Aldrich as a 1.9 M solution in 2.0 M HCl. CAPS was obtained from Sigma. All chemicals were purchased as reagent grade and used without further purification. Titanium(III) citrate was prepared in a Coy anaerobic chamber from $TiCl_3$ and sodium citrate as follows: 2.6 mL of $TiCl_3$ (in HCl) was mixed with 25 mL of a freshly prepared 0.4 M sodium citrate solution, and the pH was adjusted to 10 using saturated aqueous Na_2CO_3. The solution was then diluted with water to 50 mL, making the final concentrations 0.1 M Ti(III) and 0.2 M citrate.

A 0.1 M CAPS buffer at pH 10.4 was prepared by dissolving 2.21 g of CAPS and 0.2 g of solid NaOH in 100 mL of water. Reduction of native F_{430} was carried out in the Coy anaerobic chamber by mixing 175 μL of CAPS buffer, 25 μL of F_{430} (5 mM), and 50 μL of titanium-

(11) Stolzenberg, A. M.; Stershic, M. T. *Inorg. Chem.* **1987**, *26*, 3082−3083.
(12) Stolzenberg, A. M.; Stershic, M. T. *J. Am. Chem. Soc.* **1988**, *110*, 6391−6402.
(13) Stolzenberg, A. M.; Stershic, M. T. *J. Am. Chem. Soc.* **1988**, *110*, 5397−5403.
(14) Renner, M. W.; Furenlid, L. R.; Barkigia, K. M.; Forman, A.; Shim, H. K.; Simpson, D. J.; Smith, K. M.; Fajer, J. *J. Am. Chem. Soc.* **1991**, *113*, 6891−6896.
(15) Renner, M. W.; Furenlid, L. R.; Stolzenberg, A. M. *J. Am. Chem. Soc.* **1995**, *117*, 293−300.
(16) Sullivan, E. P., Jr.; Grantham, J. D.; Thomas, C. S.; Strauss, S. H. *J. Am. Chem. Soc.* **1991**, *113*, 5264−5270.
(17) Kratky, C.; Angst, C.; Johansen, J. E. *Angew. Chem., Int. Ed. Engl.* **1981**, *20*, 211−212.
(18) Procyk, A. D.; Stolzenberg, A. M.; Bocian, D. F. *Inorg. Chem.* **1993**, *32*, 627−633.
(19) Procyk, A. D.; Bocian, D. F. *Inorg. Chem.* **1993**, *32*, 366−367.
(20) Rospert, S.; Voges, M.; Berkessel, A.; Albracht, S. P. J.; Thauer, R. K. *Eur. J. Biochem.* **1992**, *210*, 101−107.
(21) Holliger, C.; Pierik, A. J.; Reijerse, E. J.; Hagen, W. R. *J. Am. Chem. Soc.* **1993**, *115*, 5651−5656.
(22) Lexa, D.; Momenteau, M.; Mispelter, J.; Savéant, J. M. *Inorg. Chem.* **1989**, *28*, 30−35.
(23) Kadish, K. M.; Franzen, M. M.; Han, B. C.; Araullo-McAdams, C.; Sazou, D. *J. Am. Chem. Soc.* **1991**, *113*, 512−517.
(24) The F_{430} crystal structure reported was actually of the 12,13-diepimer $F_{430}Me_5$ bromide salt; EXAFS results for 12,13-diepimer $F_{430}Me_5$ and F_{430}-Me_5 are identical.
(25) Shiemke, A. K.; Shelnutt, J. A.; Scott, R. A. *J. Biol. Chem.* **1989**, *264*, 11236−11245.
(26) Shiemke, A. K.; Kaplan, W. A.; Hamilton, C. L.; Shelnutt, J. A.; Scott, R. A. *J. Biol. Chem.* **1989**, *264*, 7276−7284.
(27) Furenlid, L. R.; Renner, M. W.; Fajer, J. *J. Am. Chem. Soc.* **1990**, *112*, 8987−8989.
(28) Wang, S.; Zhang, H.; Scott, R. A. Unpublished results.
(29) Suh, M. P.; Kim, H. K.; Kim, M. J.; Oh, K. Y. *Inorg. Chem.* **1992**, *31*, 3620−3625.
(30) Suh, M. P.; Lee, Y. J.; Jeong, J. W. *J. Chem. Soc., Dalton Trans.* **1995**, 1577−1581.
(31) Furenlid, L. R.; Renner, M. W.; Szalda, D. J.; Fujita, E. *J. Am. Chem. Soc.* **1991**, *113*, 883−892.
(32) Szalda, D. J.; Fujita, E.; Sanzenbacher, R.; Paulus, H.; Elias, H. *Inorg. Chem.* **1994**, *33*, 5855−5863.
(33) Ram, M. S.; Riordan, C. G.; Ostrander, R.; Rheingold, A. L. *Inorg. Chem.* **1995**, *34*, 5884−5892.
(34) Hamilton, C. L.; Ma, L.; Renner, M. W.; Scott, R. A. *Biochim. Biophys. Acta* **1991**, *1074*, 312−319.

(III) citrate (in this order). This solution was transferred to the EPR tube and diluted with ethylene glycol as glassing agent (~55% v/v), yielding samples with a final F_{430} concentration of ~0.25 mM. The samples were removed from the anaerobic chamber and frozen immediately in liquid nitrogen.

Preparation of Ni^{I}OEiBC. OEiBC and Ni^{II}OEiBC were synthesized as previously described.[35] The as-synthesized 1:1 mixture of *ttt* and *tct* OEiBC isomers was separated by liquid chromatography as described by Sullivan *et al.*[16] Ni^{II}OEiBC was converted to the Ni(I) form by reduction with 0.1% Na−Hg amalgam in 2-Me-THF that had been distilled under nitrogen from sodium benzophenone, as previously described.[15] EPR/ENDOR samples were ~0.5 mM. The Ni(I) forms of both the *ttt*/*tct* isomers and of pure *tct* gave identical EPR/ENDOR results; the spectra shown are for pure *tct*-Ni^{I}OEiBC.

EPR and ENDOR Studies. CW "Q"-band (35 GHz) EPR/ENDOR spectra were recorded on a modified Varian E-109 spectrometer. Pulsed Q-band and X-band (~9.5 GHz) spectra were recorded on locally-built spectrometers that have been previously described.[36−38] All CW Q-band EPR/ENDOR spectra were recorded at 2 K and in dispersion mode, under "rapid-passage" conditions.[36,39,40] CW ^{14}N ENDOR signals were enhanced by application of rf broadening as described previously.[41] Pulsed ENDOR spectra were recorded at either 2 or 4.2 K using either the Mims[42] or Davies[43] pulse sequences. The specific sequence and attendant pulse width/delay times were selected to optimize signal using the following criteria. The Mims sequence has "blind spots" for hyperfine couplings when A (MHz) $= n/\tau_{1,2}$ (μs), $n = 1, 2, ...$[44] However, for typical values of $\tau_{1,2} \approx 200$ ns, $A < 5$ MHz can be detected without interference of blind spots. Such small hyperfine couplings are commonly observed for ^{2}H,[45] and many types of ^{1}H. Larger hyperfine couplings ($A > 8$ MHz), such as those for ligand ^{14}N and some types of ^{1}H, require the Davies sequence. In this sequence, the ENDOR response depends on the product of A and the preparation pulse width t_p, with the maximum intensity at A (MHz) $\times$ t_p (μs) $\approx$ 0.7.[37,43,45,46] Thus $t_p = 0.04$ μs was chosen so as to enhance the ^{14}N X-band Davies ENDOR signals ($A(^{14}N) = 25-30$ MHz; $At_p \approx 1$) while suppressing the overlapping ^{1}H pattern ($A(^{1}H) \leq 5$ MHz; $At_p < 0.2$).

As described by Doan *et al.*,[45] we employed the following procedure to compare quantitatively pulsed ENDOR spectra. The absolute ENDOR effect is the change in echo height (in mV) for a given applied rf. This is converted to a relative ENDOR effect by dividing by the echo height in the absence of rf for Mims ENDOR or in the absence of the preparation pulse for Davies ENDOR. This relative ENDOR effect allows comparison between spectra obtained under the same conditions (pulse widths, g values, etc.) for different samples, *e.g.*, cofactor in H_2O versus D_2O buffer.

The single-crystal ENDOR transition frequencies for a nucleus, J, of spin $I = {}^1/_2$ (e.g., ^{1}H, ^{13}C, ^{15}N) are given to first order by eq 1:[47]

$$\nu_{\pm} = |\nu_J \pm A^J/2| \quad (1)$$

where A^J is the orientation-dependent nuclear hyperfine coupling constant and ν_J is the nuclear Larmor frequency. If $\nu_J > A^J/2$, as is usually the case for protons in biological systems, then the ENDOR spectrum consists of a hyperfine-split doublet centered about the Larmor frequency. For $\nu_J < A^J/2$, as is the case for nuclei with small nuclear Larmor frequencies, then the ENDOR spectrum consists of a Larmor-split doublet centered at $A^J/2$. For a quadrupolar nucleus, J, with $I \geq 1$ (e.g., ^{14}N, $I = 1$) the ENDOR pattern is further split into $2I$ lines with the frequencies given to first order by eq 2:[39,47]

$$\nu_{\pm}(m) = |\nu_J \pm A^J/2 + 3P^J(2m - 1)/2| \quad (2)$$

where $-I + 1 \leq m \leq I$. This splitting is governed by P^J, the orientation-dependent quadrupole coupling constant. Computer simulation and analysis of frozen-solution ENDOR spectra employed procedures and a program (GENDOR) described elsewhere.[39,48,49] For the analysis of ^{14}N ENDOR spectra, the equations derived by Muha were used,[50] as incorporated into our simulation software. An ENDOR simulation program, DDPOWHE, was also used that performs exact calculation of transition energies and probabilities by matrix diagonalization.[51]

In addition to the magnetic parameters, ENDOR spectral simulations require line width parameters. Simulations of Ni^{I}OEiBC X- and Q-band ^{14}N spectra employed a Gaussian ENDOR line width of 0.5 MHz (hwhm), which exactly reproduces the line width observed at g_1. A Gaussian ENDOR line width of 0.8 MHz was employed for the $Ni^{I}F_{430}$ spectra. EPR line width effects can lead to broadening and/or observation of additional resonances due to contributions from neighboring orientations (g_{obs} values).[52] These effects were found to be insignificant here, with the sole exception being the Ni^{I}OEiBC ^{14}N spectrum at g_3, wherein the orientation selection is hampered by the small field separation from g_2. Simulations using GENDOR incorporating a very small EPR line width (10 MHz) reproduced the observed high-frequency shoulder. Computer simulation of EPR spectra employed the program QPOWA.[53]

Results

EPR of $Ni^{I}F_{430}$ and Ni^{I}OEiBC. We have prepared $Ni^{I}F_{430}$ (strain ΔH) by aqueous Ti(III) citrate reduction and recorded its Q-band EPR spectrum at 2 K. As noted above, the spectrum was obtained under adiabatic rapid passage conditions and so appears as the absorption line shape (not shown). To aid in comparison with traditional, absorption-mode EPR at X-band, Figure 2A shows the numerical first derivative spectrum with the abscissa plotted as g value. The spectrum still appears axial at this higher microwave frequency, even in a numerical second derivative (not shown). There is no resolved ^{14}N hyperfine splitting at Q-band and, as shown by Figure 2B, the spectrum can be simulated using an axial $\boldsymbol{g}$ tensor: $g_{\|} = 2.244$, $g_{\perp} = 2.063$; axial single-crystal line widths, $W_{\|} = 140$, $W_{\perp} = 90$ MHz. This Q-band EPR result is in agreement with the previous X-band study of $Ni^{I}F_{430}$ (strain Marburg) reduced by aqueous Ti(III) citrate which gave $g_{\|} = 2.224$, and $g_{\perp} = 2.061$, but also exhibited ^{14}N hyperfine coupling with $a_{iso}(^{14}N) = 1.0$ mT (29 MHz at $g_{\perp}$).[21] The slight difference in $g_{\|}$ is likely the result of the glassing agent (55% v/v ethylene glycol) used to obtain relaxation properties suitable for ENDOR ($Ni^{I}F_{430}$ in aqueous buffer alone gave very weak and poorly resolved ENDOR signals).

(35) Stolzenberg, A. M.; Spreer, L. O.; Holm, R. H. *J. Am. Chem. Soc.* **1980**, *102*, 364−370.
(36) Hoffman, B. M.; Gurbiel, R. J.; Werst, M. M.; Sivaraja, M. In *Advanced EPR. Applications in Biology and Biochemistry*; Hoff, A. J., Ed.; Elsevier: Amsterdam, 1989; pp 541−591.
(37) Fan, C.; Doan, P. E.; Davoust, C. E.; Hoffman, B. M. *J. Magn. Reson.* **1992**, *98*, 62−72.
(38) Davoust, C. E.; Doan, P., E; Hoffman, B. M. *J. Mag. Reson., A* **1996**, *119*, 38−44.
(39) Hoffman, B. M.; DeRose, V. J.; Doan, P. E.; Gurbiel, R. J.; Houseman, A. L. P.; Telser, J. In *EMR of Paramagnetic Molecules*; Biological Magnetic Resonance; Berliner, L. J., Reuben, J., Eds.; Plenum Press: New York, 1993; Vol. 13, pp 151−218.
(40) Hoffman, B. M. *Acc. Chem. Res.* **1991**, *24*, 164−170.
(41) Hoffman, B. M.; DeRose, V. J.; Ong, J. L.; Davoust, C. E. *J. Magn. Reson.* **1994**, *110*, 52−57.
(42) Mims, W. B. *Proc. R. Soc. London* **1965**, *283*, 452−457.
(43) Davies, E. R. *Phys. Lett.* **1974**, *47A*, 1−2.
(44) Gemperle, C.; Schweiger, A. *Chem. Rev.* **1991**, *91*, 1481−1505.
(45) Doan, P. E.; Fan, C.; Hoffman, B. M. *J. Am. Chem. Soc.* **1994**, *116*, 1033−1041.
(46) Doan, P. E.; Fan, C.; Davoust, C. E.; Hoffman, B. M. *J. Magn. Reson.* **1991**, *95*, 196−200.
(47) Abragam, A.; Bleaney, B. *Electron Paramagnetic Resonance of Transition Ions*, 2nd ed.; Clarendon Press: Oxford, U.K., 1970.
(48) Hoffman, B. M.; Martinsen, J.; Venters, R. A. *J. Magn. Reson.* **1984**, *59*, 110−123.
(49) Hoffman, B. M.; Venters, R. A.; Martinsen, J. *J. Magn. Reson.* **1985**, *62*, 537−542.
(50) Muha, G. M. *J. Magn. Reson.* **1982**, *49*, 431−443.
(51) Telser, J.; Smith, E. T.; Adams, M. W. W.; Conover, R. C.; Johnson, M. K.; Hoffman, B. M. *J. Am. Chem. Soc.* **1995**, *117*, 5133−5140.
(52) Brown, T. G.; Hoffman, B. M. *Mol. Phys.* **1980**, *39*, 1073−1109.
(53) Belford, R. L.; Belford, G. G. *J. Chem. Phys.* **1973**, *59*, 853−854.

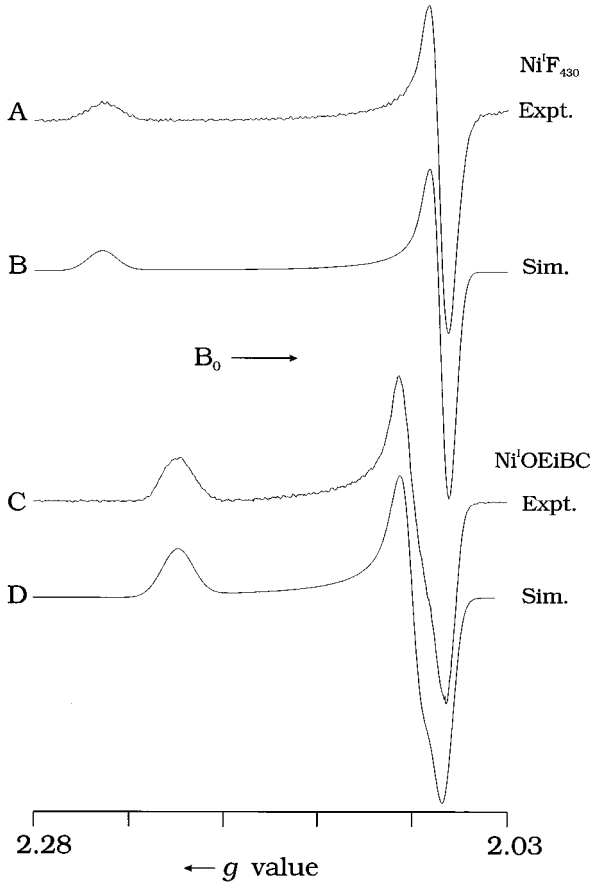

Figure 2. Experimental (A, C) and simulated (B, D) Q-band EPR spectra of (A) Ni^{I}F$_{430}$ generated by reduction of F$_{430}$ using Ti(III) citrate and of (C) Ni^{I}OEiBC generated by reduction of Ni^{II}OEiBC using Na amalgam in 2-Me-THF. The spectra were recorded using the dispersion mode under passage conditions; a numerical first derivative is shown. The abscissa is in g value to facilitate comparison between spectra. (A) Experimental conditions: sample concentration, ~0.25 mM in 0.1 M, pH = 10.4 CAPS buffer with 55% (v/v) ethylene glycol; temperature, 2 K; microwave frequency, 35.035 GHz; microwave power, 2 μW (50 dBm); 100 kHz field modulation amplitude, 0.1 mT; time constant, 32 ms. (B) Simulation parameters: $g_{\|} = 2.244$, $g_{\perp} = 2.063$; $W_{\|} = 90$ MHz, $W_{\perp} = 140$ MHz. (C) Experimental conditions: sample concentration, ~0.5 mM in 2-Me-THF; temperature, 2 K; microwave frequency, 35.422 GHz; microwave power, 2 mW (20 dBm); 100 kHz field modulation amplitude, 0.03 mT; time constant, 32 ms. (D) Simulation parameters: $g_x = 2.063$, $g_y = 2.080$, $g_z = 2.204$; $W_{x,y} = 100$ MHz, $W_z = 155$ MHz.

The Q-band EPR spectrum of Ni^{I}OEiBC at 2 K is shown in Figure 2C, together with a simulation, shown in Figure 2D, generated using a rhombic **g** tensor with **g** = [2.204, 2.080, 2.063]; $W_1 = 155$ MHz, $W_{2,3} = 100$ MHz. As with Ni^{I}F$_{430}$, no ^{14}N hyperfine splitting was observed nor included in the Q-band simulation. The **g** tensor is in agreement with the X-band EPR spectrum reported for Ni^{I}OEiBC (see Table 1), but which exhibited resolved ^{14}N hyperfine splitting with $a_{iso}(^{14}N) = 0.98$ mT (28 MHz at g_3).[15] As has been shown extensively for Cu(II) complexes, lower microwave frequencies (lower magnetic fields) can be preferable for resolving hyperfine coupling, while higher microwave frequencies are desirable for resolving **g** anisotropy.[54]

The **g** tensors for Ni^{I}F$_{430}$ and Ni^{I}OEiBC are characteristic of $S = {}^1/_2$ d^9 "square-planar" (pseudo-D_{4h}) complexes wherein the direction of $g_{\|}$ (g_1) is normal to the macrocycle plane and that of $g_{\perp}$ ($g_{2,3}$ for rhombic systems) lies in the plane.[55] As summarized in Table 1, the magnitudes of these g values correspond closely to those of tetraaza macrocyclic complexes of Ni(I) and Cu(II) with varying degrees of ligand unsaturation.[52,56]

Table 1. Electronic (**g** Tensor) Parameters for d^9 Macrocyclic Complexes

complex	$g = [g_1, g_2, g_3]$[a]	ref
Ni^{I}F$_{430}$	2.244, 2.063, 2.063[b]	this work
	2.224, 2.061, 2.061[c]	ref 21
Ni^{I}F$_{430}$12,13-diepimer	2.238, 2.057, 2.057	ref 21
Ni^{I}F$_{430}$Me$_5$	2.250, 2.074, 2.065	ref 66
Ni^{I}F$_{430}$(NH-*n*-Bu)$_5$	2.244, 2.076, 2.060	ref 34
Ni^{I}OEiBC	2.204, 2.080, 2.063[b]	this work
	2.2025, 2.083, 2.061[c]	ref 15
Ni^{I}Me$_6$[14]1,4,8,11-tetraeneN$_4$	2.195, 2.053, 2.053	ref 56
Ni^{I}Me$_6$[14]4,11-dieneN$_4$	2.226, 2.055, 2.055	ref 56
Cu^{II}TPP	2.190, 2.045, 2.045	ref 52
Cu^{II}OEiBC	2.206, 2.048, 2.048[b]	ref 86

[a] The direction of g_1 is normal to the macrocycle plane; the other two components lie in-plane. [b] Determined at Q-band; no ^{14}N hyperfine coupling resolved. [c] Determined at X-band; ^{14}N hyperfine coupling resolved.

^{1,2}H ENDOR of Ni^{I}F$_{430}$ and ^{1}H ENDOR of Ni^{I}OEiBC. The Q-band CW ^{1}H ENDOR spectra of Ni^{I}F$_{430}$ in H$_2$O and D$_2$O buffer recorded at magnetic field positions corresponding to $g_{\|}$ each show several resolved ^{1}H doublets (see eq 1) as seen in Figure 3, parts A and B, respectively. None of the resolved features is lost in D$_2$O buffer, demonstrating that there are no solvent-exchangeable hydrogens with significant hyperfine coupling. This is supported by spectra obtained at $g_{\perp}$ using both CW and pulsed (Mims) ^{1}H ENDOR techniques (data not shown). Further support comes from pulsed (Mims) ^{2}H ENDOR of Ni^{I}F$_{430}$ in D$_2$O buffer (Figure S1, Supporting Information), which allows direct investigation of the solvent-exchangeable resonances. This shows only a very narrow ^{2}H ENDOR signal at both $g_{\perp}$ and $g_{\|}$ (total breadth (hwhm) < 0.3 MHz) associated with deuterons of outer-coordination sphere solvent. This is in agreement with the earlier X-band ESEEM study of Ni^{I}F$_{430}$ in D$_2$O buffer by Holliger *et al.*, which also found no measurable ^{2}H hyperfine coupling; only a signal arising from many, relatively distant (4−8 Å) D$_2$O molecules was observed.[21]

Figure 3C shows the CW ^{1}H ENDOR spectrum for Ni^{I}OEiBC in 2-Me-THF solution at $g_{\|}$. Signals from several magnetically inequivalent protons are evident, although there appears to be fewer types of proton resonances, as expected. Spectra at multiple field positions (not shown) indicate that the sharp signals at $A(^1H) = 1.6$ MHz are relatively isotropic while the broad shoulders, which maximize to $A(^1H) \approx 7.5$ MHz at $g \approx 2.15$, are very anisotropic.

^{14}N ENDOR of Ni^{I}F$_{430}$ and Ni^{I}OEiBC. Both Ni^{I}OEiBC and Ni^{I}F$_{430}$ exhibit strong ^{14}N ENDOR signals over the rf range 5−25 MHz at both X- and Q-band microwave frequencies. Figure 4 displays the ENDOR spectra recorded at the "single-crystal-like" field position corresponding to $g_{\|}$ (g_1) for Ni^{I}OEiBC at Q-band (Figure 4A) and at X-band (Figure 4B), and for Ni^{I}F$_{430}$ at X-band (4C). The corresponding spectrum for Ni^{I}F$_{430}$ at Q-band is shown in Figure S2A. For each complex, the Q-band ^{14}N ENDOR spectrum is a four-line pattern consisting of a $\nu_{\pm}$ doublet of doublets. These doublets are centered at $A(^{14}N)/2 \approx 14$ MHz and separated by $2\nu(^{14}N) \approx 7$ MHz as given by eq 1 (Figures 4A and S2A); the subdoublet

(54) Hyde, J. S.; Froncisz, W. *Ann. Rev. Biophys. Bioeng.* **1982**, *11*, 391−417.

(55) Pilbrow, J. R. *Transition Ion Electron Paramagnetic Resonance*; Clarendon Press: Oxford, U.K., 1990.

(56) Lovecchio, F. V.; Gore, E. S.; Busch, D. H. *J. Am. Chem. Soc.* **1974**, *96*, 3109−3118.

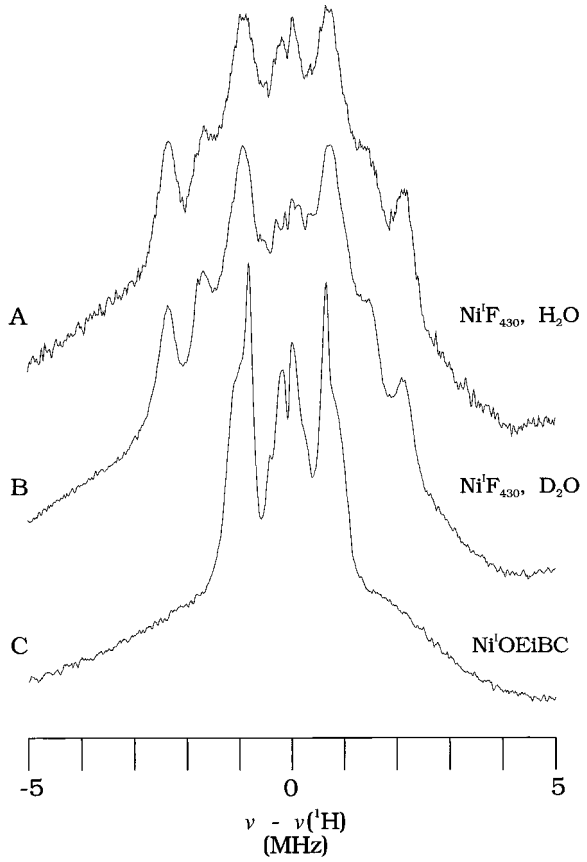

Figure 3. Q-band CW ^{1}H ENDOR spectra of Ni^{I}F$_{430}$ in H_2O (A) and D_2O buffer (B) and of Ni^{I}OEiBC in 2-Me-THF (C). The spectra have been centered at the ^{1}H Larmor frequency ($\nu_H \approx 55$ MHz) to facilitate comparison between spectra. Experimental conditions: (A) temperature, 2 K; microwave frequency, 35.035 GHz; microwave power, 6 μW (45 dBm); magnetic field, 1.1160 T ($g = 2.243$, $g_{||}$); 100 kHz field modulation amplitude, 0.03 mT; time constant, 32 ms; rf scan rate, 0.25 MHz/s; average rf power, 5 W, applied in a 20% duty cycle square wave at a 10 kHz repetition rate; 50 scans. (B) as in A except: microwave frequency, 35.004 GHz; magnetic field, 1.1150 T ($g = 2.243$, $g_{||}$); 60 scans. (C) as in A except: microwave frequency, 35.255 GHz; microwave power, 200 μW (30 dBm); 100 kHz field modulation amplitude, 0.07 mT; rf scan rate, 0.5 MHz/s; eight scans; magnetic field, 1.1430 T ($g = 2.204$, g_1). The relative spectral intensities are arbitrary.

splitting is ~1.5 MHz for Ni^{I}OEiBC and ~2.1 MHz for Ni^{I}F$_{430}$. At X-band, the pattern again is centered at ~14 MHz but has collapsed to a triplet because of the 4-fold decrease in ν(^{14}N).

There are two alternate interpretations of a $\nu_{\pm}$(^{14}N) doublet of doublets at g_1. One is that the signal is from a single ^{14}N hyperfine coupling, with $\nu_{\pm}$ branches further split into doublets by the quadrupole interaction as given by eq 2 for ^{14}N ($I = 1$). The second is that the pattern is the sum of offset doublets with slightly differing hyperfine couplings, neither associated with an observable quadrupole splitting. This second case would require that the unresolved quadrupole splitting along g_1, the normal to the macrocycle plane, be $|P_{g1}| < 0.2$ MHz for *both* of the two types of nitrogen ligand. This value is low in comparison with analogous macrocyclic complexes such as Cu^{II}TPP[52] and high-spin aquometmyoglobin.[57] ENDOR studies of all of these showed quadrupole couplings of $|P_{g1}| \approx 0.3$ MHz (see Table 2). Thus, on the basis of prior studies, it seems unlikely that the pattern in Figure 4A arises from two types of nitrogen with unresolved quadrupole splitting.[58]

(57) Scholes, C. P.; Lapidot, A.; Mascarenhas, R.; Inubushi, T.; Isaacson, R. A.; Feher, G. *J. Am. Chem. Soc.* **1982**, *104*, 2724−2735.

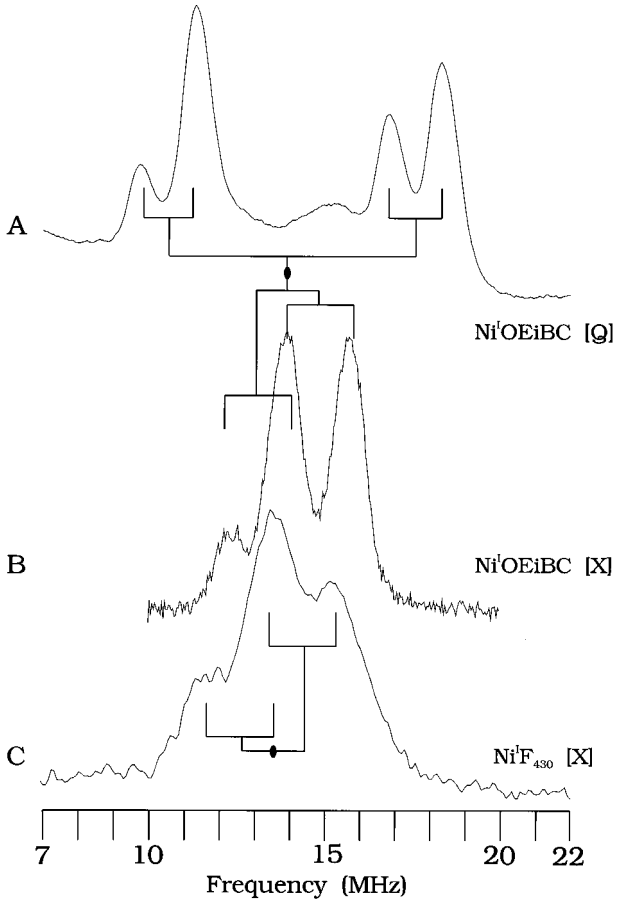

Figure 4. Experimental ^{14}N ENDOR spectra of Ni^{I}OEiBC in 2-Me-THF at Q-band (A) and at X-band (B) and of Ni^{I}F$_{430}$ in D_2O buffer at X-band (C). Experimental conditions: (A) temperature, 2 K; microwave frequency, 35.255 GHz; microwave power, 2 mW (20 dBm); magnetic field, 1.143 T ($g = 2.20$); 100 kHz field modulation amplitude, 0.3 mT; time constant, 32 ms; rf scan rate, 1.5 MHz/s; average rf power, 5 W, applied in a 20% duty cycle square wave at a 10 kHz repetition rate; 10 scans; (B) temperature, 4.2 K; microwave frequency, 9.58 GHz; magnetic field, 0.311 T ($g = 2.20$, g_1); Davies sequence, π microwave pulse width (t_p), 40 ns; τ_{23}, 166 ns; rf pulse width (t_{rf}), 20 μs; rf power, 400 W (3−0 dB); repetition rate, 12.5 Hz; (C) temperature, 4.2 K; microwave frequency, 9.41 GHz; magnetic field, 0.302 T ($g = 2.22$, $g_{||}$); Davies sequence, π microwave pulse width (t_p), 40 ns; τ_{23}, 262 ns; rf pulse width (t_{rf}), 20 μs; rf power, 400 W (3−0 dB); repetition rate, 20 Hz. A(^{14}N)/2 is indicated by ●. The crossbars passing near ● indicate twice the ^{14}N Larmor frequency (2ν(^{14}N) ≈ 7 MHz at Q-band; 2 MHz at X-band). The "goal posts" indicate the quadrupole splitting, $3P \approx$ 1.5−2 MHz in all cases.

To explore fully the properties of the pyrrole-^{14}N ligands, ENDOR patterns were recorded at numerous field positions across the EPR envelope so as to determine the ^{14}N hyperfine and quadrupole coupling tensors and distinguish between the two alternative interpretations of the spectra at g_1. The resulting "2-D" data set for Ni^{I}OEiBC at Q-band is shown in Figure 5 and at X-band in Figure S3; data for Ni^{I}F$_{430}$ at Q-band is given in Figure S2 and at X-band in Figure S4. The data set for Ni^{I}OEiBC at Q-band (Figure 5) is the most informative in large part because of the enhanced orientation selection conferred by rhombic splitting in its EPR spectrum (Figure 2C) but also because the ENDOR resolution is higher than that for Ni^{I}F$_{430}$

(58) Furthermore, preliminary Q-band CW ENDOR data for Cu^{II}OEiBC in 2-Me-THF solution show a similar ^{14}N pattern at $g_{||}$ consisting of $\nu_{\pm}$ branches each further split by ~2 MHz.[86] In contrast to Ni^{I}OEiBC, the Cu(II) complex shows no evidence for inequivalence among the pyrrole nitrogen ligands,[15] so that only an assignment of the subdoublet splitting to quadrupole coupling is reasonable.

Table 2. Magnetic Parameters for Pyrrole Nitrogen Ligands in Paramagnetic Macrocyclic Complexes

complex		$\mathbf{A} = [A_1, A_2, A_3]$ (MHz)[a]	$\mathbf{P} = [P_1, P_2, P_3]$ (MHz)[a]
Ni^{I}OEiBC	$N_{1,3}$[b]	33.0(5), 29.0(5), 28.0(0.2)	−1.50(10), 0.95(10), 0.55(5)
	$N_{2,4}$[b]	35.0(5), 27.0(5), 28.0(0.2)	−1.00(10), 0.45(10), 0.55(5)
$Ni^{I}F_{430}$	$N_{1,3}$[c]	31(1), 22(1), 26.5(0.5)	−1.85(20), 1.10(20), 0.75(5)
	$N_{2,4}$[c]	34(1), 27(1), 26.5(0.5)	−1.35(20), 0.60(20), 0.75(5)
Cu^{II}TPP[d]		54.213, 42.778, 44.065	−0.619, 0.926, −0.307
Fe^{III}Heme (Mb)[e]		49.30, 34.45, 35.55[f]	−0.77, 1.04, −0.27

[a] The single-crystal metalloporphyrin studies show that $\mathbf{A}(^{14}N)$ and $\mathbf{P}(^{14}N)$ are collinear, with A_1 and P_1 along the metal−nitrogen bond, A_2 and P_2 in-plane, normal to the metal-nitrogen bond, and A_3 and P_3 normal to the macrocycle plane. [b] In 2-Me-THF solution; this work. [c] In aqueous ethylene glycol (∼55% v/v) solution; this work. [d] Doped into Zn^{II}TPP single crystal.[52] [e] Aquometmyoglobin (high-spin ferric) single-crystal.[57] [f] Obtained by multiplying the reported values by five, so that the values determined for $S = {}^5/_2$ aquometmyoglobin are converted to a hypothetical $S = {}^1/_2$ system.

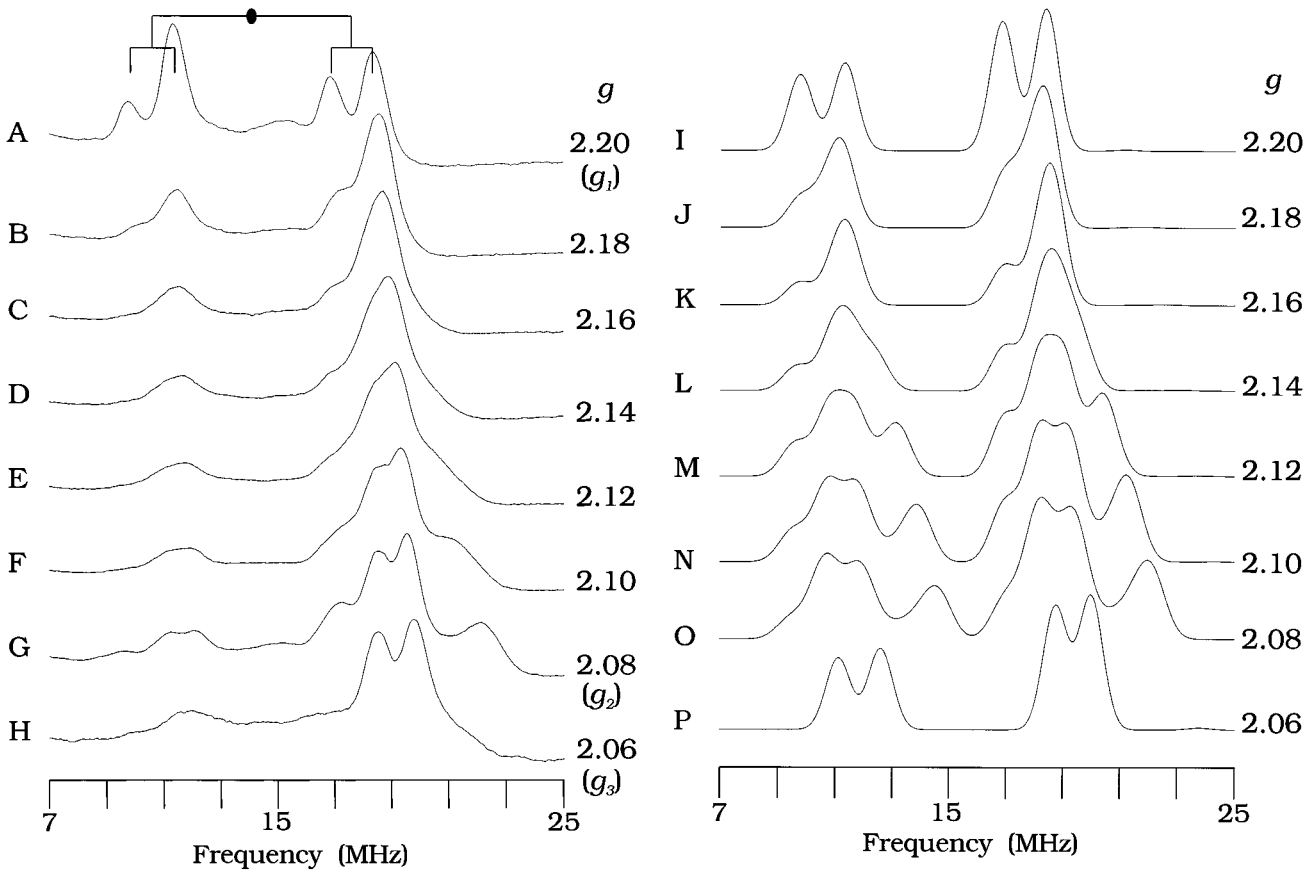

Figure 5. Experimental Q-band CW (A−H) and simulated (I−P) ^{14}N ENDOR spectra of Ni^{I}OEiBC in 2-Me-THF. Experimental conditions as in Figure 4A, except the magnetic field was (A) 1.143 T ($g = 2.20$); (B) 1.1555 T ($g = 2.18$); (C) 1.166 T ($g = 2.16$); (D) 1.177 T ($g = 2.14$); (E) 1.188 T ($g = 2.12$); (F) 1.1995 T ($g = 2.10$); (G) 1.211 T ($g = 2.08$); (H) 1.223 T ($g = 2.058$). $A(^{14}N)/2$ is indicated by ●. The crossbar passing through ● indicates twice the ^{14}N Larmor frequency ($2\nu(^{14}N) = 7.0$ MHz at g_1). The "goal posts" indicate the quadrupole splitting, $3P$. Simulation parameters, $\boldsymbol{g} = [2.204, 2.080, 2.063]$, and equal contribution of two types of ^{14}N as follows: $\mathbf{A}(^{14}N_{1,3}) = [33.0, 29.0, 28.0]$ MHz, $\mathbf{P}(^{14}N_{1,3}) = [-1.50, 0.95, 0.55]$ MHz, **A** and **P** tensors rotated with respect to $\boldsymbol{g}$ tensor by Euler angles: $\alpha_{1,3} = 0$, $\beta_{1,3} = 90°$, $\gamma_{1,3} = 45°$; $\mathbf{A}(^{14}N_{2,4}) = [35.0, 27.0, 28.0]$ MHz, $\mathbf{P}(^{14}N_{2,4}) = [-1.00, 0.45, 0.55]$ MHz, $\alpha_{2,4} = 0°$, $\beta_{2,4} = 90°$, $\gamma_{2,4} = 135°$; ENDOR line width, 0.5 MHz (Gaussian, hwhm); EPR line width, 10 MHz (Gaussian, hwhm).

at Q-band. The increased resolution likely is a consequence of the better glass formed by the organic versus aqueous solvent, which reduces spin diffusion and increases relaxation times for solute paramagnets.

The ν_+ and ν_- branches of the ^{14}N pattern observed for Ni^{I}OEiBC at g_1 (Figure 5A) can be followed across the EPR envelope with ν_+ being more intense at most fields, as is often the case.[36] The overall center of the pattern, the effective $A(^{14}N)/2$, changes little. However, the nature of the pattern changes markedly with field. For example, focusing on ν_+, a shoulder appears to higher frequency as the field is increased from g_1 toward g_2, becomes a resolved peak at g_2 (2.08), then retreats to lower frequency at the high field edge of the spectrum. This is the result of significant anisotropy in the hyperfine coupling and/or in the quadrupole coupling; the latter is traceless and thus *necessarily* anisotropic. A similar situation, albeit with poorer resolution, is obtained for $Ni^{I}F_{430}$ (Figure S2).

We begin our analysis with the assumption that the low-field ($g_1 = 2.20$) signal arises from the $\nu_\pm$ branches of a ^{14}N ENDOR signal in which the four pyrrole nitrogens of Ni^{I}OEiBC and $Ni^{I}F_{430}$ are indistinguishable.[59] This assignment leads to the values for couplings normal to the macrocycle plane, $A_3(^{14}N_{1-4})$ and $P_3(^{14}N_{1-4})$ (see Chart 2), listed in Table 2. The labeling of the tensor component directions (*i.e.*, A_3, $P_3(^{14}N_i)$ along g_1) is chosen to correspond with the studies of porphyrin and other systems.[60]

(59) We use the term pyrrole here, although in these reduced porphyrins, the term pyrrole/pyrroline is more appropriate.

Chart 2

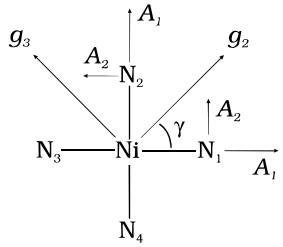

To understand the field dependence, first consider the high-field ($g_3 = 2.06$) single-crystal-like spectrum of Ni^{I}OEiBC (Figure 5H). Comparing this spectrum with that at low-field ($g_1 = 2.20$) (Figure 5) reveals that these two "edge" spectra exhibit quite similar subdoublet splittings of the ν_+ branch; likewise, the X-band spectrum at g_3 is a triplet (Figure S3F), just as seen at g_1 (Figures 4B and S3A). Once again, the spectrum at g_3 can be described as resulting either from two overlapping ^{14}N patterns, both without quadrupole splitting, or from one type of ^{14}N with quadrupole splitting. To distinguish between these alternatives, consider the diagram in Chart 2 for a NiN_4 unit viewed down the g_1 (A_3, P_3) axis. The in-plane **g** tensor axes are related to the molecular frame by the angle γ: for $\gamma = 0°$, the **g** and molecular (nuclear) coordinate systems are collinear; for $\gamma = 45°$, $g_{2,3}$ bisect the N−Ni−N bond angles. Studies on porphyrinic systems have shown that the ^{14}N hyperfine tensor is expected to be roughly axial with the direction of maximum hyperfine coupling (A_1) lying along the metal−nitrogen bond. The hyperfine and quadrupole coupling tensors are collinear with one in-plane principal quadrupole direction along the metal−nitrogen bond vector (P_1) and the other, the largest magnitude coupling, normal to the metal−nitrogen bond (P_2) so that $\mathbf{P}(^{14}N) \approx [-0.7, 1, -0.3]$ MHz (relevant coupling constants are summarized in Table 2).[52,57] However, as shown in metal-coordinated imidazole and pyridine, the largest quadrupole coupling (∼1−1.6 MHz) often lies along the metal−nitrogen bond.[61−63]

If the $P_i(^{14}N)$ magnitudes for Ni^{I}OEiBC are close to those for porphyrins and other complexes with nitrogen heterocycles, as is shown below to be the case, then the spectrum at g_3 is strong evidence for $\gamma \approx 45°$. First, there is *no* value of γ that can give negligible quadrupole coupling for both pairs of *trans* nitrogen ligands (*i.e.*, $|P_{obs}| \leq 0.2$ for both $N_{1,3}$ and $N_{2,4}$; see Chart 2), so an interpretation in terms of two different nitrogens with $P_{obs} \approx 0$ is ruled out. For example, if the in-plane **g** tensor directions were collinear with the Ni−N bonds ($\gamma = 0°$), then at g_3, one set of nitrogens would have $\mathbf{B}_0$ parallel to Ni−N and $P_{obs} = P_2$; the other would have $P_{obs} = P_1$. The resulting ENDOR pattern would contain *two* superimposed four-line ($\nu_\pm$ doublet of doublet) patterns. The pattern must then reflect a symmetry equivalence among *all* nitrogens for this orientation. The only way to obtain a *single* quadrupole splitting when $\mathbf{B}_0$ lies along g_3 (a single $\nu_\pm$ quartet) is to have $\gamma \approx 45°$.

For a **g** tensor rotation of $\gamma = 45°$, the hyperfine coupling observed at g_3 is $A_{g3}(^{14}N_i) = [\{A_1(^{14}N_i)^2 + A_2(^{14}N_i)^2\}/2]^{1/2} \approx$ 31 MHz. Determining the individual in-plane hyperfine components requires consideration of spectra taken where *both* are independently contributing to the observed pattern, namely when the magnetic field is directed along a Ni(I)−N bond vector, (see Chart 2). For $\gamma = 45°$, this occurs at $g = \{(g_2^2 + g_3^2)/2\}^{1/2} = 2.072$. In fact, although EPR line width effects make spectra taken at $g = 2.080$ (g_2), 2.075, and 2.070 almost identical, resolution is slightly better at $g = 2.075$, as predicted. Again focusing on the ν_+ branch, at $g = 2.08$ (Figure 5G), one sees four resolved features; an almost identical, albeit less intense, pattern is seen for the ν_- branch. General consideration of the expected patterns indicates that these peaks should be assigned as two doublets, one from each pair of *trans* nitrogens ($^{14}N_{1,3}$ and $^{14}N_{2,4}$), one pair with subdoublet splitting $3P_1$, and the other with $3P_2$. There are, however, several independent ways in which the four $\nu_\pm$ peaks can be paired to yield two doublets, two of which, {*ac*, *bd*} and {*ab*, *cd*}, correspond to permissible quadrupole couplings.[64] Combining this with the condition for $\gamma = 45°$ that $A_{g3}(^{14}N_i) = [\{A_1(^{14}N_i)^2 + A_2(^{14}N_i)^2\}/2]^{1/2} \approx 31$ MHz gives two trial solutions for the $\mathbf{A}(^{14}N)$ and $\mathbf{P}(^{14}N)$ tensors. Computer simulation shows that the entire field-dependent ^{14}N ENDOR pattern can be reproduced using refined values of *both* sets of coupling tensors, as given in Table 2.[60] We note that γ may not vary more than ∼2° from 45° in order to preserve the observed resolution.

Given that the full ^{14}N ENDOR data set can be described by a single type of pyrrole ^{14}N with *either* set of coupling tensors given in Table 2, then it is of course possible to describe the data set by the superposition of spectra from equal contributions from the two types of ^{14}N. In fact, the EXAFS data indicate that there are two types of nitrogen ligand in equal abundance. We therefore present in Figure 5I−P simulations generated by summing equally these two types of nitrogen, which match the overall patterns and resonant frequencies quite well across the entire EPR envelope; note that the details of experimental CW ENDOR intensities are quite difficult to reproduce since they are dependent on complex relaxation effects.[36,39,40]

To test the analysis, the X-band spectra also were examined. In this case, the ^{14}N ENDOR pattern consists of overlapping resonances from the ν_+ and ν_- branches, making it impractical to analyze the field-dependent data set independently. However, X-band spectra are indeed well matched by simulations calculated as superimposed spectra from the two sets of magnetic parameters determined by analysis of the Q-band spectra (Figures S3G−L).[65] This correspondence of the ^{14}N ENDOR spectra taken at two microwave frequencies confirms the essential validity of the pyrrole-^{14}N coupling tensors in Table 2 with the in-plane $g_{2,3}$ axes bisecting the N−Ni−N bond angles ($\gamma = 45°$).

The ^{14}N ENDOR data for Ni$^{I}F_{430}$, in particular pulsed (Davies) 35 GHz ENDOR at 2 and 4.2 K, clearly exhibit the same characteristics as Ni^{I}OEiBC, despite the poorer resolution of the Q-band signals (Figures S2 and S5). However, because the $\boldsymbol{g}$ tensor for Ni$^{I}F_{430}$ is axial, no in-plane orientation selection occurs, which severely reduces the ability to detect differences among the pyrrole nitrogen ligands. Nevertheless, the peak

(60) Positive $A_i(^{14}N)$ values are expected on the basis of numerous studies as summarized in Brown and Hoffman.[52] In their doped single-crystal ENDOR study of Cu^{II}TPP, second-order quadrupole splitting effects were observed that allowed assignment of the signs of P_1 and P_2 relative to A_1 and A_2, respectively, so that P_1 was negative and P_2 was positive (P_3 was negative, but was determined from the constraint that $P_1 + P_2 + P_1 \equiv 0$).[52] These effects are not observable in this frozen-solution ENDOR study, so there is no independent basis for the assignment of an absolute sign to $P(^{14}N)_{g1}$. However, the quadrupole analysis (see below) allows absolute signs of P_i to be assigned.

(61) Hsieh, Y. N.; Rubenacker, G. V.; Cheng, C. P.; Brown, T. L. *J. Am. Chem. Soc.* **1977**, *99*, 1384−1389.

(62) Ashby, C. I. H.; Cheng, C. P.; Brown, T. L. *J. Am. Chem. Soc.* **1978**, *100*, 6057−6063.

(63) Ashby, C. I. H.; Cheng, C. P.; Duesler, E. N.; Brown, T. L. *J. Am. Chem. Soc.* **1978**, *100*, 6063−6067.

(64) At $g = 2.075$, the ν_+ branch exhibits resolved peaks at 17.2 (*a*), 18.5 (*b*), 19.6 (*c*), and 22.3 (*d*) MHz. The pairing *ad*, *bc* gives $|P| \approx 1.7$ and 0.3 MHz, respectively, which when combined with $|P_3| = 0.55$ MHz cannot give a traceless **P** tensor. However, the pairing *ac*, *bd* gives $|P| \approx$ 0.8 and 1.3 MHz, respectively, and the pairing *ab*, *cd* gives $|P| \approx 0.4$ and 0.9 MHz, respectively, both of which satisfy this requirement.

(65) Despite the use of pulsed techniques to suppress the overlapping ^{1}H resonances (see the Experimental Section), some residual contribution to the ^{14}N ENDOR pattern likely remains at $\nu_H \approx 13-14$ MHz.

positions and pattern breadth at $g_\perp$ can be analyzed in a manner similar to that for Ni^{I}OEiBC at $g_{2,3}$ and the spectra can be interpreted equally well in terms of two types of nitrogen (parameters given in Table 2). Computer simulations employing equal sums of spectra calculated with these two parameter sets are successful at reproducing the field-dependent pattern, as shown in Figure S2. Equally important, as shown in Figure S4, the X-band ^{14}N pattern is well reproduced using the magnetic parameters determined from the Q-band analysis.

Discussion

EPR Spectra of Ni(I) Macrocyclic Complexes. Both axial and slightly rhombic EPR spectra are observed for Ni(I) macrocyclic complexes, and no generalizations based on ligand or solvent can be made. For example, aqueous Ni^{I}F$_{430}$ has an axial EPR spectrum, but Ni^{I}F$_{430}$Me$_5$, prepared using Na amalgam in THF as reductant, exhibits a slightly rhombic EPR spectrum,[66] as do Ni^{I}F$_{430}$ pentabutylamide,[34] Ni^{I}OEiBC, and other Ni(I) hydroporphryin models for Ni^{I}F$_{430}$[14] (see Table 1 for **g** tensor values). However, Ni^{I}Me$_6$[14]4,11-dieneN$_4$, prepared by electrochemical reduction in acetonitrile solution, exhibits an axial EPR spectrum,[56] although its crystal structure (as the perchlorate salt) shows two significantly different Ni(I)−N bond distances.[31]

The relation between the **g** tensor and the molecular framework for square-planar d^9 complexes, chiefly those of Cu(II), was studied theoretically a number of years ago,[67−69] and is summarized by Pilbrow.[55] Crystal-field terms of rhombic (*i.e.*, mixing of $d_{x^2-y^2}$ and d_{z^2} orbitals) and/or monoclinic (*i.e.*, mixing of d_{xz} and d_{yz} orbitals) symmetry acting via spin−orbit coupling can lead to a rhombic ***g*** tensor, as well as to rotation of the in-plane **g** tensor directions ($g_{2,3}$) relative to the molecular coordinate system. In the case of Ni^{I}OEiBC, for which a rhombic **g** tensor is observed, the ^{14}N ENDOR data clearly demonstrate that the nonaxial ligand field terms indeed rotate the **g** tensor by 45° relative to the molecular frame. However, the **g** tensor can still be axial in the presence of both rhombic and monoclinic terms if their effects are equal and opposite.[67] This is likely the case for Ni^{I}F$_{430}$, which exhibits an axial ***g*** tensor despite the ligand's nonplanar geometry (see Chart 1). Apparently these macrocyclic Ni(I) complexes represent a situation in which the several crystal-field effects are in close competition so that slight changes in ligand, solvent, etc., can alter the electronic-structure observables.

^{1,2}H ENDOR. These studies indicate the absence of axial coordination by water in the active, Ni(I) form. In contrast, numerous spectroscopic studies including EXAFS,[25,26] resonance Raman,[25,26,70] and MCD[71,72] have indicated that the isolated cofactor contains predominantly axially coordinated bis-aquo $S = 1$ Ni(II). Thus reduction of F$_{430}$ leads to the opening up of axial coordination site(s), potentially allowing reaction with substrate.

Without deuterated samples, specific assignment of the constitutive ^{1}H resonances for the two Ni(I) complexes (Figure 3B,C) is not possible. Nevertheless, we can make some comparisons between the ^{1}H ENDOR seen for these complexes with results for other tetrapyrrole systems, such as Cu^{II}TPP, also noting that the EPR spectrum of Cu^{II}TPiBC is nearly identical to that of Cu^{II}TPP.[73] The single-crystal ENDOR study of Cu^{II}TPP doped into Zn^{II}TPP determined the **A**(^{1}H) tensors for four types of magnetically equivalent pyrrole protons.[52] The average tensor corresponded to roughly **A**(^{1}H) = [3.5, 1.7, 1.2], a_{iso} = 2.13 MHz. Thus the magnitude of the largest proton couplings seen in Cu^{II}TPP for the pyrrole 3,4-hydrogens (3.5 MHz) is somewhat smaller than those seen for Ni^{I}OEiBC (3.5−7.5 MHz) and Ni^{I}F$_{430}$ (4.0−4.5 MHz). This suggests that these strongest ^{1}H couplings may correspond to the pyrroline hydrogens in Ni^{I}OEiBC and Ni^{I}F$_{430}$. Cu^{II}TPP lacks meso hydrogens; for comparison, ENDOR studies have been reported on several Fe(III) porphyrins that do contain meso hydrogens.[57] In particular, for low-spin Fe(III) systems, the meso protons gave very sharp signals with $|A_{zz}|$ = 1.4−1.2 MHz (cyano) and 1.0 MHz (azido).[57] It is thus reasonable to assign the sharp resonances seen at $g_{||}$ having $A(^1H)$ = 2 MHz in Ni^{I}F$_{430}$ and 1.6 MHz in Ni^{I}OEiBC to meso protons, realizing that spin densities on metalloporphyrins are quite sensitive to the metal ion's electronic properties.[16] Finally, the large number of more distant, side chain hydrogens presumably contribute to the large signal intensity at $A(^1H) < 1$ MHz for both Ni(I) systems, in rough analogy with the various sidechains of other tetrapyrrole ligands. For example, Godziela and Goff performed solution NMR studies on Cu^{II}OEP,[74] and from their data estimates can be made of a_{iso} for the ethyl side chain methylene and methyl protons of 0.4 and 0.07 MHz, respectively.

Finally, we note that there are solvent-exchangeable hydrogens on the side chain groups of F$_{430}$: five carboxylates, an amide, and a lactam (see Figure 1). At pH = 10.4, the carboxylates are extensively ionized and thus are unlikely to contribute to the ^{1,2}H resonances; however, the amide and lactam would remain unionized. The lactam in particular has the solvent-exchangeable hydrogen likely closest to Ni(I), and it may be contributing to the ^{2}H ENDOR signal.

^{14}N ENDOR. The ^{14}N ENDOR data have been interpreted in light of the EXAFS studies so as to describe the four nitrogen ligands of Ni^{I}OEiBC and Ni^{I}F$_{430}$ as falling into two sets, N$_{1,3}$ and N$_{2,4}$, with each set containing two *trans* nitrogens (see Chart 2). The resulting spin Hamiltonian parameters for the two types of ligand can be used to describe bonding in the Ni^{I}N$_4$ core and to compare this bonding to that in Cu^{II}TPP,[52] and other complexes (see Table 2).

By following Brown and Hoffman,[52] we consider each $A(^{14}N_i)$ tensor within the local coordinate system defined at the ligands (see Chart 2). In this coordinate system, N(p_y) is out-of-plane and N(p_z) lies along the M−N bond, with N(p_x) also in-plane. In idealized D_{2h} symmetry, the unpaired electron is in a σ-bonding MO defined as follows:

$$\Psi_{B_{1g}} = \alpha_1\phi_{d_{xy}} - \alpha_2^{1,3}[\phi^1_{2s} + \phi^3_{2s}] + \alpha_2^{2,4}[\phi^2_{2s} + \phi^4_{2s}] + \alpha_3^{1,3}[\phi^1_{2p_z} - \phi^3_{2p_z}] - \alpha_3^{2,4}[\phi^2_{2p_z} - \phi^4_{2p_z}] \quad (3)$$

We have left out any contributions from terms involving Ni(I)−N in-plane and out-of-plane π-bonding and from other atoms of the macrocycle. The former simplification is justified because the **A**(^{14}N) tensors described here are nearly axial.

(66) Jaun, B.; Pfaltz, A. *J. Chem. Soc., Chem. Commun.* **1986**, 1327−1329.
(67) Hitchman, M. A.; Olson, C. D.; Belford, R. L. *J. Chem. Phys.* **1969**, *50*, 1195−1203.
(68) Hitchman, M. A. *J. Chem. Soc. A* **1970**, *1970*, 4−9.
(69) Belford, R. L.; Harrowfield, B.; Pilbrow, J. R. *J. Magn. Reson.* **1977**, *28*, 433−439.
(70) Shiemke, A. K.; Scott, R. A.; Shelnutt, J. A. *J. Am. Chem. Soc.* **1988**, *110*, 1645−1646.
(71) Cheesman, M. R.; Ankel-Fuchs, D.; Thauer, R. K.; Thomson, A. J. *Biochem. J.* **1989**, *260*, 613−616.
(72) Hamilton, C. L.; Scott, R. A.; Johnson, M. K. *J. Biol. Chem.* **1989**, *264*, 11605−11613.
(73) Richardson, P. F.; Chang, C. K.; Hanson, L. R.; Spaulding, L. D.; Fajer, J. *J. Phys. Chem.* **1979**, *83*, 3420.
(74) Godziela, G. M.; Goff, H. M. *J. Am. Chem. Soc.* **1986**, *108*, 2237−2243.

Chart 3

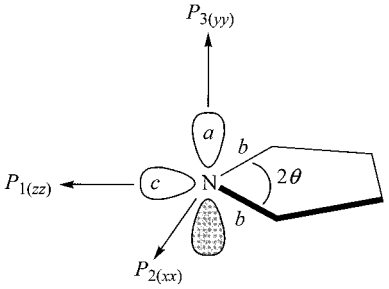

We may further simplify the picture by treating the pyrrole nitrogens as being sp^n hydridized as shown in Chart 3. The hybridization is defined in terms of the covalency parameters and, in an idealized situation, is related to the ligand geometry:[52]

$$n = \alpha_3^2/\alpha_2^2 = (1 - \cot^2\theta)/\cot^2\theta = \tan^2\theta - 1 \quad (4)$$

where 2θ is the C−N−C bond angle and crystallographically determined values for 2θ are used to determine n.[75] In this study we shall use experimentally determined bonding coefficients determined from the measured ^{14}N hyperfine tensors to calculate n and to *define* "θ_{expt}" from eq 4.

This ground state MO leads to the following expressions for the $\mathbf{A}(^{14}N)$ tensor components for a given nitrogen:[52,76]

$$A_{1(z)} = 4(\alpha_2^2 A_0 + \alpha_3^2 T_0/5) + A_{D1} \quad (5)$$

$$A_{2(x)} = 4(\alpha_2^2 A_0 - \alpha_3^2 T_0/10) + A_{D2}$$

$$A_{3(y)} = 4(\alpha_2^2 A_0 - \alpha_3^2 T_0/10) + A_{D3}$$

where the isotropic term for one electron in a ^{14}N 2s orbital is $A_0 = (g_e g_N \beta_e \beta_N/h)(2\pi/3)|\psi_0|^2 = 388.9$ MHz and the dipolar term for an electron in a ^{14}N 2p orbital is $T_0 = (g_e g_N \beta_e \beta_N/h)\cdot\langle r_p^{-3}\rangle = 116.5$ MHz, using the values for $|\psi_0|^2$ and $\langle r_p^{-3}\rangle$ tabulated by Goodman and Raynor,[77] as was done in the Cu^{II}TPP study.[52] Through-space dipolar coupling between a ^{14}N nucleus and electron spin on the Ni is represented by A_{Di} (i = 1,3).[78] Thus the isotropic hyperfine couplings, $a_{iso}(^{14}N) = 4\alpha_2^2 A_0 = 47.02$ MHz for Cu^{II}TPP and 30.0 MHz for Ni^{I}OEiBC, provide the values of α_2 given in Table 3. Use of a point−dipole approximation and an average value for R = 2.0 Å, based on EXAFS data (see below), in A_{Di}[78] gives α_1 = 0.9, as compared to 0.82 for Cu^{II}TPP. The relatively short distance of the Ni(I)−N bond makes use of the point−dipole approximation questionable; however, Snetsinger *et al.*, in a recent study of a low-spin Fe(III) system, provided equations for calculation of dipolar coupling between a ligand nucleus and spin density in a metal 3d orbital.[79] Using their method in combination with the above values for R and α_1, we obtain an estimate for the direct dipolar contribution $A_{D1} \approx 1.2$ MHz in all of these Ni(I) complexes. Solving eq 5 then yields the values for α_3 listed in Table 3.[80] The hybridization of each type of nitrogen, n, calculated from eq 4, is also given in Table 3.

Table 3. Molecular Orbital Parameters for Pyrrole Nitrogen Ligands in d^9 Porphyrinic Complexes[a]

complex	α_2	α_3	n_{expt}[b]	c[c]	a	b	N_Td
Ni^{I}OEiBC							
$N_{1,3}$	0.139	0.139	1.00	1.961	1.295	1.235	5.73
$N_{2,4}$	0.139	0.202	2.11	1.940	1.609	1.623	6.80
Ni$^{I}F_{430}$							
$N_{1,3}$	0.130	0.188	2.09	1.948	1.354	1.302	5.90
$N_{2,4}$	0.137	0.196	2.05	1.943	1.490	1.513	6.46
Cu^{II}TPP[e]	0.174	0.252	2.106	1.906	1.751	1.568	6.79

[a] See text for explanation of parameters. [b] Calculated from $n = \alpha_3^2/\alpha_2^2$. [c] Calculated from $c = 2 - (\alpha_2^2 + \alpha_3^2) = 2$ for free ligand. [d] Calculated from $N_T = c + a + 2b = 5$ for neutral nitrogen atom. [e] These values do not include the nitrogen 1s contribution.[52] They are scaled to correspond with the MO definition given in eq 3.

The quadrupole interaction provides information on the overall distribution of charge in the nitrogen orbitals, rather than just the unpaired electron distribution. A modified version of the Townes−Dailey model can be used to interpret ^{14}N quadrupole tensors.[52,61,63] This model uses a coordinate system identical to that described above for the hyperfine coupling (see Chart 3) and gives the following expressions for the diagonal components of the quadrupole coupling tensor:

$$P_{1(zz)} = P_0[c(1 - \cot^2\theta) - a/2 + b(-^1/_2 + \cot^2\theta)] \quad (6)$$

$$P_{2(xx)} = P_0[-(c/2)(1 - \cot^2\theta) - a/2 + (b/2)(2 - \cot^2\theta)]$$

$$P_{3(yy)} = P_0[-(c/2)(1 - \cot^2\theta) + a - (b/2)(1 + \cot^2\theta)]$$

where c is the population of the nitrogen lone pair orbital (c = 2 for the free ligand), a is the N $p\pi$ orbital population, and b is the population of each N−C bonding orbital. A quadrupole coupling for a single 2p electron in atomic N of $e^2qQ/h = 2P_0 = -9.0$ MHz is commonly used,[52,61,62] which gives $\mathbf{P} = [-3.0, 1.5, 1.5]$ MHz for an idealized sp^2 nitrogen ($2\theta = 120°$). As described above, we use an experimental value for 2θ defined through eq 4. This leaves the three orbital population parameters, a, b, and c, to be determined. Because **P** is traceless, the three P_i components provide only two independent experimental parameters; moreover the relative signs of these components are determined by experiment, but the absolute signs are not.[60] However, these difficulties are easily overcome. The covalency parameters determined from the ^{14}N hyperfine tensor give c: $c = 2 - (\alpha_2^2 + \alpha_3^2)$.[52] This then allows eq 6 to be solved using either of the two choices of absolute sign for the P_i components, which are found to have the form: $\pm[-|P_1|, +|P_2|, +|P_3|]$. Choice of the negative sign gives $a, b > 2$, which is physically meaningless; whereas the positive sign in all cases gives orbital occupancy values comparable to those seen for Cu^{II}TPP and other systems. The final results for the two types of N for both Ni(I) complexes, as well as those for CuTPP, are summarized in Table 3. The sum of the individual orbital occupancies then gives the overall orbital population of nitrogen, $N_T = c + a + 2b$.

Examination of the orbital coefficients determined from the ^{14}N hyperfine and quadrupole coupling allows comparison of bonding in these Ni(I) complexes to Cu^{II}TPP and other species.

(75) For Cu^{II}TPP, $2\theta = 108°$, which gives $n = 0.89$.[52] Similar values for n result using the 2θ values for the structurally characterized Ni(II) analogues. For Ni^{II}OEiBC,[17] the average $2\theta = 107.0(5)°$, giving $n = 0.83$; for Ni$^{II}F_{430}Me_5$,[9] ring A has $2\theta = 112.0°$ giving $n = 1.20$; and rings B, C, and D have average $2\theta = 108.5(5)°$, giving $n = 0.93$.

(76) Rist, G. H.; Hyde, J. S. *J. Chem. Phys.* **1969**, *50*, 4532−4542.

(77) Goodman, B. A.; Raynor, J. B. In *Advances in Inorganic Chemistry and Radiochemistry*; Emeléus, H. J., Sharpe, A. G., Eds.; Academic Press: New York, 1970; Vol. 13, pp 135−362.

(78) These terms are given by the following: $A_{D1(z)} = 2g_\perp(g_N\beta_e\beta_N/h)\alpha_1^2[R^{-3} + (6/7)R^{-5}\langle r_{d_{xy}}^2\rangle]$; $A_{D2(x)} = -g_\perp(g_N\beta_e\beta_N/h)\alpha_1^2[R^{-3} + {}^3/_7R^{-5}\langle r_{d_{xy}}^2\rangle]$; $A_{D3(y)} = -g_\parallel(g_N\beta_e\beta_N/h)\alpha_1^2[R^{-3} + {}^9/_7R^{-5}\langle r_{d_{xy}}^2\rangle]$, where R is the metal−nitrogen distance and $\langle r_{d_{xy}}^2\rangle$ is the expectation value for the metal d_{xy} orbital, and terms in R^{-7} are left out.[52,76]

(79) Snetsinger, P. A.; Chasteen, N. D.; van Willigen, H. *J. Am. Chem. Soc.* **1990**, *112*, 8155−8160.

(80) We note that even use of $A_{D1} = 1.6$ MHz, an extreme upper bound derived from $R = 1.9$ Å and $\alpha_1 = 1$, only changes α_3 slightly, from 0.20 to 0.19 in the case of Ni^{I}OEiBC $N_{2,4}$.

The experimentally determined hybridization at nitrogen is quite close to sp^2 in all cases, except for $N_{1,3}$ of Ni^{I}OEiBC, where n is only 1, close to the crystallographic value.[75] The net σ-electron donation from a single coordinated nitrogen to the metal ion is given by the sum of bonding coefficients, $\alpha_2^2 + \alpha_3^2$. The charge donation values so obtained for $N_{2,4}$ of Ni^{I}OEiBC and for both types of N in $Ni^{I}F_{430}$ are roughly 60% of that in Cu^{II}TPP; $N_{1,3}$ of Ni^{I}OEiBC has a σ-donation only 40% that of Cu^{II}TPP. The lesser covalency, corresponding to lesser N → M donation, is not surprising given the poorer energy match between the nitrogen $2sp^2$ and metal 3d orbitals of Ni(I) compared to Cu(II), as indicated by considering valence-shell ionization energies.[81]

The quadrupole couplings manifest the lesser covalence for Ni(I) in an interesting fashion. As pointed out by Brown and Hoffman,[52] for M−N complexes the largest ^{14}N quadrupole coupling is either negative and along the M−N bond (lone pair) direction or positive and normal to the M−N bond (in-plane). Using a series of Zn(II) and Cd(II) pyridine complexes, Hsieh *et al*. showed that a switch from the first to the second case occurs as the nitrogen lone pair-to-metal donation increases (*c* decreases),[61] and the switch has indeed occurred for Cu^{II}TPP and aquometmyogblobin (see Table 2). In contrast, for these Ni(I) complexes, the N → M donation is too small to induce this shift, so that the direction and sign of largest quadrupole coupling corresponds to that of the free ligand.

The ligand-only orbital occupancies (*a* and *b*) of $N_{2,4}$ of Ni^{I}OEiBC (and to a lesser extent, $N_{2,4}$ of $Ni^{I}F_{430}$) resemble those of the pyrrole ligands in Cu^{II}TPP, while $N_{1,3}$ of Ni^{I}OEiBC do not, nor does $N_{1,3}$ of $Ni^{I}F_{430}$. Interestingly, these nitrogen ligands have similarities with the imine nitrogen of metal-coordinated imidazole. Analysis of NQR data for a series of Zn(II) imidazole complexes[62,63] gives orbital occupancy parameters that resemble those for $N_{1,3}$ of both Ni(I) complexes.[82] Consistent with this, the maximum hyperfine anisotropy (defined as $(|A_{max}| - |A_{min}|)/a_{iso}$) of Cu(II)-coordinated imidazole in $Ag^{I}{}_2Cu^{II}{}_2$ bovine SOD is ∼15%,[83] the same as that for $N_{1,3}$ of Ni^{I}OEiBC, while for Cu^{II}TPP and $N_{2,4}$ of Ni^{I}OEiBC and $N_{2,4}$ of $Ni^{I}F_{430}$, there is ∼25% anisotropy.

The choice of the wave function in eq 3 expressly ignores contribution to the ^{14}N hyperfine coupling by π-bonding with the metal, and this is a good approximation. However, one may qualitatively note that such π-bonding is manifested by the slightly rhombic $\mathbf{A}(^{14}N)$ tensor ($A_3 \neq A_2$).[84] For Cu^{II}TPP, $(A_3 - A_2) = 1.3$ MHz, which is similar to that for $N_{2,4}$ in Ni^{I}OEiBC (1 MHz), suggesting common characteristics for the π bonding. However, for $N_{1,3}$ and both types of nitrogen in $Ni^{I}F_{430}$, $(A_3 - A_2)$ differs significantly from ∼1 MHz, suggesting differences in π bonding, which might be caused by deviations from planarity in the macrocyclic ligand (see Chart 1).

Comparison of EPR/ENDOR and EXAFS Results. EXAFS and crystallographic studies have been performed on several OEiBC and F_{430} species,[9,15,17,27] as well as on numerous Ni(II) porphyrins.[85] Both Ni^{II}OEiBC and Cu^{II}OEiBC in THF showed four equivalent M−N distances (1.94 Å for Ni(II)−N; 2.00 for Cu(II)−N),[15] and the crystal structure of *tct*-Ni^{II}OEiBC likewise gave a single average Ni(II)−N bond length of 1.942 Å.[17] EXAFS studies of Ni^{I}OEiBC in THF, however, showed inequivalent nitrogen ligands in that pairs of nitrogen atoms with two Ni(I)−N distances were required to fit the data: 1.91 and 2.07 Å.[15]

EXAFS studies showed a similar difference between the Ni(II) and Ni(I) forms of F_{430}. As-isolated F_{430} (*i.e.*, $S = 1$, pseudo-octahedral with axially coordinated bis aquo ligands) was analyzed using equivalent Ni(II)−N distances of 2.10 Å,[25,26] and $F_{430}Me_5$ (*i.e.*, $S = 0$, square-planar) had equivalent Ni(II)−N distances of 1.90(2) Å,[27] in agreement with the average Ni(II) distance determined from its crystal structure: 1.86(2).[9] However, this contrasts with the EXAFS results for both $Ni^{I}F_{430}Me_5$ in THF and aqueous $Ni^{I}F_{430}$; two sets of Ni(I)−N distances were required: 1.88(3) and 2.03(3) Å for the former,[27] and 1.90(3) and 2.04(3) Å for the latter.[28] As mentioned above, the presence of two Ni(I)−N distances in several tetraaza macrocyclic complexes has been confirmed by x-ray crystallography.[29,30,32,33,56] In particular, for $Ni^{I}Me_6$[14]4,11-dieneN$_4$ both a crystal structure and EXAFS studies have been performed and are in excellent agreement: the crystal structure gave a Ni(I)−N_{amine} distance of 2.066(6) Å and Ni(I)−N_{imine} distance of 1.984(7) Å, and EXAFS in acetonitrile solution gave 2.06(2) and 1.97(2) Å, respectively.[31] This expansion and distortion of the NiN_4 core has been rationalized by the ability of these relatively flexible macrocyclic ligands to accommodate the larger Ni(I) ion, with radius $r \geq 2.1$ Å compared to square-planar Ni(II) with $r = 1.9$ Å.[12−14]

The EXAFS results for $Ni^{I}F_{430}$ and Ni^{I}OEiBC give two sets of Ni(I)−N bonds lengths differing by ∼8% (∼0.15 Å), well outside the experimental error (∼1%). The X-band EPR spectra of both $Ni^{I}F_{430}$ and Ni^{I}OEiBC exhibited resolved hyperfine coupling from the four nitrogen ligands at $g_\perp$ but did not indicate any magnetic inequivalence among them.[15,21] The present ENDOR studies at X- and Q-bands give average ^{14}N hyperfine coupling constants in good agreement with the EPR-determined values ($Ni^{I}F_{430}$, $a_{iso} = 28$ MHz; Ni^{I}OEiBC, $a_{iso} = 30$ MHz), but they also support a model employing two types of nitrogen ligand. The in-plane hyperfine coupling for these two types of ligand differs by ∼2 MHz out of ∼30 MHz, or roughly 7%. Interpretation of the hyperfine and quadrupole coupling tensors for these two types of nitrogen shows quite noticeable electronic differences between them (see Table 3) wherein one set of nitrogen ligands in these Ni(I) complexes is similar to the pyrrole nitrogen ligands in Cu^{II}TPP and the other is not, but with parameters resembling the imine nitrogen of metal-coordinated imidazole.

Conclusions

We have performed EPR and ENDOR studies using pulsed and CW techniques at X- and Q-band microwave frequencies on $Ni^{I}F_{430}$, the putative active state of the methylreductase enzyme,[7,8,20] and parallel studies on Ni^{I}OEiBC, which has been used extensively as a model for $Ni^{I}F_{430}$.[11−15] The EPR results reported here at Q-band agree with those reported earlier at X-band.[21] The Q-band EPR spectrum of $Ni^{I}F_{430}$ is rigorously axial in aqueous solution: $g_\parallel = 2.244$, $g_\perp = 2.063$. In contrast, Ni^{I}OEiBC in 2-Me-THF exhibits a slight rhombicity: $\mathbf{g} = 2.204$,

(81) Ballhausen, C. J.; Gray, H. B. In *Molecular Orbital Theory*; W. A. Benjamin, Inc.: New York, 1965; Chapter 8.

(82) Typical values for a series of bis and tetrakis imidazole complexes of Zn(II) (calculated using Figures 2−4, Table 4, and text material in the study by Ashby *et al.*[62]) are as follows: $c = 1.70$, $a = 1.15$, $b = 1.05$, and $N_T = 4.95$. These workers determined *c* by a linear correlation between h/e^2qQ and η. $N_{1,3}$ of Ni^{I}OEiBC fits this correlation reasonably well giving $c \approx 1.87(3)$, as does $N_{1,3}$ of $Ni^{I}F_{430}$, which gives $c \approx 1.93(5)$, while $N_{2,4}$ of both complexes does not, nor does Cu^{II}TPP.

(83) Gurbiel, R. J.; Peoples, R.; Doan, P. E.; Cline, J. F.; McCracken, J.; Peisach, J.; Hoffman, B. M.; Valentine, J. S. *Inorg. Chem.* **1993**, *32*, 1813−1819.

(84) There is also a slight rhombic contribution to $\mathbf{A}(^{14}N)$ from the direct dipolar coupling, which arises from anisotropy in $\mathbf{g}$ and in $\langle r_{d_{xy}}{}^2 \rangle$ (see Brown and Hoffman[52] and Snetsinger *et al.*[79]); however, this contribution is small in these systems: $|A_{D2} - A_{D3}| \leq 0.1$ MHz.

(85) Barkigia, K. M.; Renner, M. W.; Furenlid, L. R.; Medforth, C. J.; Smith, K. M.; Fajer, J. *J. Am. Chem. Soc.* **1993**, *115*, 3627−3635.

(86) Telser, J.; Renner, M. W.; Hoffman, B. M. Unpublished results.

2.080, 2.063. Previous work has shown that both the $Ni^{I}F_{430}$ pentamethyl ester and the pentabutyl amide also show rhombic EPR spectra.[34,66] However, other tetraazamacrocyclic Ni(I) species show axial EPR spectra in organic solvent.[56] Apparently, the electronic structure of Ni(I) species is quite sensitive to ligand conformational and solvation effects. For Ni^{I}OEiBC, ^{14}N ENDOR shows that the in-plane **g** tensor components are directed exactly between the bonds ($\gamma = 45°$) resulting from strong in-plane ligand field effects at the metal. This result has been often found for Cu(II) chelate complexes and is now shown to be the case for a Ni(I) complex.

In the resting state, the $S = 1$ Ni(II) ion has axial bis-aquo coordination as shown by Raman and MCD studies.[25,26,71,72] In contrast, the Ni(I) active state shows no evidence of coordination by water, as shown by this ^{1,2}H ENDOR study and in earlier ESEEM work.[21] Thus, reductive activation of F_{430} *in vivo* may open the axial site(s) to coordination by the substrate, CH_3SCoM, as found here *in vitro*.

EXAFS studies of $Ni^{I}F_{430}$,[28] $Ni^{I}F_{430}Me_5$,[27] and Ni^{I}OEiBC[15] show two sets of Ni(I)−N bond distances, differing by ∼8%. This is presumably the source of the ligand field effects detected by EPR/ENDOR. For both Ni^{I}OEiBC and $Ni^{I}F_{430}$, the ^{14}N ENDOR data can be interpreted as resulting from the superposition of two types of nitrogen ligand in equal abundance, consistent with the EXAFS results. Analysis of the hyperfine and quadrupole coupling parameters for these two types of nitrogen shows substantial differences in bonding to Ni(I): one type of nitrogen ligand resembles the pyrrole nitrogen of Cu^{II}TPP, while the other has some similarities with the imine nitrogen of Zn(II) imidazole complexes.

One can anticipate that theoretical studies of spin distribution, making use of the EXAFS and ENDOR data and comparison with the better understood porphyrin systems, might be able to correlate the effects of not only the small differences in Ni(I)−N bond distances, but also the spatial alignment of the nitrogen ligands with respect to the macrocycle plane. ENDOR studies of other macrocyclic Ni(I) complexes will be undertaken as well to provide a larger data base on this interesting class of coordination complexes.

Acknowledgment. This work was supported by grants from the NSF (DMB-8907559 to B.M.H., MCB-9013276 to R.A.S., a Research Opportunity Award to J. T., and Research Training Group Award DIR-9014281 to the Center for Metalloenzyme Studies) and from the Department of Energy, Chemical Sciences Division (Contract DE-AC02−76CH00016). We thank Dr. Peter E. Doan for assistance with the pulsed ENDOR measurements and helpful comments.

Supporting Information Available: Five supporting figures referred to in the text (10 pages). See any current masthead page for ordering and Internet access instructions.

JA9625337